


Thickness-dependent neutralization of low-energy alkali-metal ions scattering on graphene

Yuanqing Shi, Liyuan Yin, Bin Ding, Xiaoxun Song, Luyao Zhang, Yanling Guo, Lin Chen^{✉,*} and Ximeng Chen[†]
*School of Nuclear Science and Technology; Key Laboratory of Special Function Materials and Structure Design, Ministry of Education;
 and Frontiers Science Center for Rare Isotopes, Lanzhou University, Lanzhou 730000, China*

Julia A. Melkozerova, A. L. Klavsyuk, and Ivan K. Gainullin[✉]
Faculty of Physics, Moscow State University, Leninskie gory 1 #2, Moscow 119992, Russia

Vladimir A. Esaulov
*Institut des Sciences Moléculaires d'Orsay and CNRS, UMR 8214, Institut des Sciences Moléculaires d'Orsay, Orsay ISMO,
 Bâtiment 351, Université-Paris Saclay, Orsay 91405, France*

 (Received 18 August 2021; revised 6 March 2022; accepted 30 March 2022; published 13 April 2022)

A challenging effort is under way to understand the essence of the quantum size effect of two-dimensional materials in order to achieve the ultimate goal of arbitrarily tailoring their properties in the near future. Here we present experimental and theoretical study of resonant neutralization of low-energy alkali-metal ions on clean and graphene-covered polycrystalline copper surfaces. The ion neutralization strongly depends on the number of graphene layers, and it gradually saturates for three to five layers of graphene. This result is consistent with that for the graphite surface. The neutral fraction for the clean polycrystalline copper surface is found to be significantly higher than that for the graphene-covered surface, which is not consistent with known regularities. We quantitatively explain those observations through the small energy level width of resonant electron transfer that is determined by the special electronic structure of graphene layers. This finding indicates that resonant neutralization spectroscopy has promising applications in the detection of the quantum size effects of two-dimensional materials at an atomic layer level.

DOI: [10.1103/PhysRevA.105.042807](https://doi.org/10.1103/PhysRevA.105.042807)

I. INTRODUCTION

Two-dimensional (2D) materials have opened possibilities for energy storage [1,2], photocatalytic activities [3], superconductivity [4], electromagnetic interference shielding [5], strong light-matter interactions [6] and new technology applications in field effect transistors [7], wearable flexible devices [8], artificial intelligence [9], radiation detectors [10], and desalination [11]. When the size of a nanocrystal is smaller than the de Broglie wavelength, electrons and holes are spatially confined and electric dipoles are formed, and discrete electronic energy level can be formed in all materials. This is the so-called quantum size effects [12]. Changes in electronic structure that scale with the size of the materials can strongly contribute to their outstanding chemical and physical properties [13–16]. A challenging effort is therefore under way to understand the essence of the quantum size effect in order to achieve the ultimate goal of arbitrarily tailoring 2D materials' properties in the near future. Here, we report that resonant neutralization spectroscopy based on the low-energy ion scattering (LEIS) technique is a promising candidate for detecting the variation of electronic structure with the number of layers in 2D materials.

LEIS is a highly sensitive surface technique and often used for surface element and structure analysis [17], like single atom catalysts [18] and topological insulator surfaces [19]. Charge transfer is involved in many aspects of technology applications, including LEIS [17], secondary ion mass spectroscopy (SIMS) [20], neutral beam heating of fusion plasma [21], high-current negative ion sources for spallation neutron sources [22], and detection of low-energy neutrals in interplanetary and interstellar space [23]. Resonant charge transfer (RCT) occurs on the metallic surfaces when the LEIS technique is performed, in which the special projectiles need to be carefully chosen. This physical phenomenon is rapidly applied to detect local electrostatic potential [24] and internal polarization [25] at bulk surfaces, and quantum confined states for supported clusters [26,27], using the alkali-metal ions.

Alkali-metal ions as incident particles for LEIS can probe the electronic structure near the surface Fermi level through measuring the proportion of alkali-metal ions that are neutralized after scattering on the surfaces [24–34]. The RCT of alkali-metal ions on jelliumlike metal surfaces is usually treated in the free-electron gas model or the jellium model. The RCT occurs when there is sufficient overlap between the *ns* level of alkali-metal ions and the conduction band of the metal surface so that electrons can transfer [29–32], and it strongly depends on ion energy level position relative to the Fermi level of the metal surface. Normally, smaller work functions lead to larger neutral fraction, and vice versa.

*chenlin@lzu.edu.cn

†chenxm@lzu.edu.cn

There are open questions about the basic physics of 2D materials, particularly with respect to their electronic properties, which must be understood in order to fully exploit their potential. In this work, we first report on the experimental study of 2–5 keV Na^+ ions in specular scattering on graphene layers grown on polycrystalline copper (PC), and compare the results with those of PC and highly oriented pyrolytic graphite (HOPG).

The measurement described here directly probes the electronic structure near the Fermi level of graphene layers by the means of the RCT processes using the ion scattering technique. The advantage of grazing scattering lies in that it avoids the penetration of incident particles into the graphene layers. The bare PC surface is the same as that used as the substrate of graphene growth. It is found that the neutral fraction decreases as the number of graphene layers increases, reaching a limiting value for three to five layers, which is the same as that scattered from HOPG. In particular, there is a sharp drop in neutral fraction for the monolayer graphene on a PC surface with lower work function, which is helpful to tune the substrate effect on the energy band structure of the freestanding graphene. The substrate effect is related to the interaction between the substrate and the graphene layer leading to the electron transfer from the substrate to the graphene [35].

II. EXPERIMENT

The experiments were performed in an ultrahigh-vacuum (UHV) experimental setup (base pressure 2×10^{-8} Pa) that is described in detail elsewhere [33]. Briefly, the Na^+ ion beam with energy range from 2 to 5 keV was produced in a homemade Na^+ ion gun, and then collimated by several slits to the beam size of $1 \times 3 \text{ mm}^2$. The incident Na^+ ions collided with the sample and the scattered particles passed through the slits, and their charge states were analyzed by a parallel-plate electrostatic deflector. Measurements were performed for specular scattering conditions (scatter angle = 7° ; incident angle = exit angle = 3.5°). The charge-state separated particles were then recorded by a one-dimensional position sensitive microchannel plate (PSMCP) detector. The PSMCP detector consists of two 56-mm-diameter microchannel plates (MCPs) stacked in a chevron configuration and mounted above a $56 \times 11 \text{ mm}^2$ strip-type resistive anode. The face of the first MCP was at ground potential and the resistive anode was kept at 2200 V at which the measured count rate became independent of pulse height. The detector efficiency for particles with different charge states is assumed to be identical at fixed energies [36–38]. A multiparameter acquisition system (MPA-3) (FAST ComTec) was used for data collection. The neutral fraction is defined as $N(\text{Na}^0)/N(\text{Na}^0 + \text{Na}^+)$ where $N(\text{Na}^0)$ and $N(\text{Na}^+)$ are the number of scattered particles corresponding to two separated peaks recorded by the PSMCP detector.

Graphene grows on copper foils of $50 \mu\text{m}$ thickness by the chemical vapor deposition method. The graphene grows directly on the surface by chemical vapor deposition and the coverage area is larger than 95%. Figure 1 shows the Raman spectra for different numbers of graphene layers. The two most intense features are the G peak at 1581 cm^{-1} and

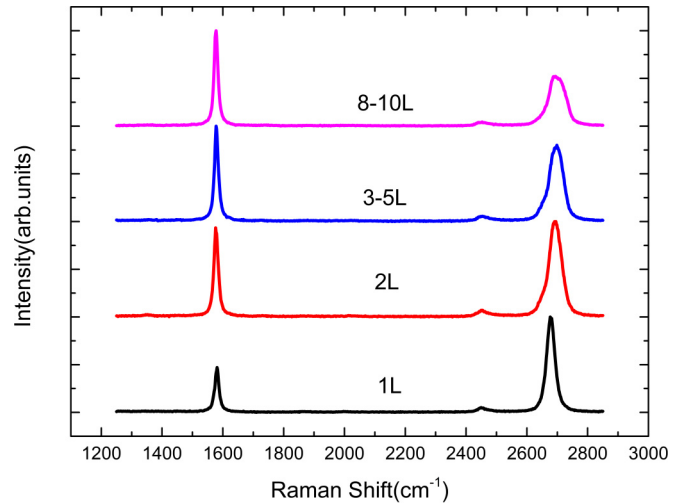


FIG. 1. Raman spectrum of graphene of different layers.

the $2D$ peak at 2680 cm^{-1} . The I_G/I_{2D} value of monolayer graphene is about $1/2$. The I_G/I_{2D} gradually increases with an increase in the number of graphene layers, and the $2D$ peak position shifts to the right and increases in width. The G -band frequency of the Raman spectra of graphene is proportional to the inverse of the layer number [39], which can determine the thickness of the graphene layers. Moreover, there is no D peak at 1350 cm^{-1} , which proves the absence of a significant number of defects.

The manufacturer quoted a mosaicity of less than 0.8° for HOPG. To obtain an atomically flat and contaminant-free surface, the layered structure of the HOPG surface simplified the preparation procedure by removing several top layers with adhesive tape. The fresh surface was then transferred immediately to the UHV chamber and prepared by annealing at about 670 K for 4 h.

In situ preparation of the PC surfaces consisted of many cycles of 3 keV Ar^+ sputtering with a beam density of $2.0 \mu\text{A}/\text{cm}^2$ and subsequent annealing at about 770 K (20 min) using electron bombardment. During sputtering, the sample was periodically moved along the direction parallel and perpendicular to the beam to ensure that the entire surface was exposed to the beam uniformly. Surface cleanliness was then verified by time-of-flight scattering and recoiling spectroscopy using 3 keV Ar^+ ions scattering on the PC surface with a scattering angle of 18° .

III. DESCRIPTION OF THE THEORETICAL APPROACH

In Sec. III, we describe the calculations of the work function and the partial density of states (PDOS) for these surfaces by the means of the Vienna *ab initio* simulation package (VASP) [40,41], as well as the calculations of the ion level width and the population of the atomic state by the wave packet propagation (WPP) method and the rate equation, respectively.

The work function and the PDOS for these surfaces were calculated using a plane-wave basis set and the plane pseudopotential wave (PAW) formalism at the level of the local density approximation, implemented in the VASP. The cutoff

energy for the expansion of wave functions and potentials in the plane-wave basis was chosen to be 500 eV, and the Brillouin zone was sampled by using a $(2 \times 5 \times 1)$ Γ -centered k -point grid for relaxation calculations and a $(2 \times 7 \times 1)$ one for static calculations. The tolerance for the energy convergence is 10^{-5} eV. The atomic relaxation was continued until the Hellmann-Feynman forces were less than 0.02 eV/Å. The vacuum layer in the supercell used in our calculations is set to be 20 Å, which is enough to minimize the artificial interlayer interactions.

According to the x-ray diffraction analysis of the PC samples under investigation, Cu(311) is the main crystal face and thus is chosen as the representative one in the calculation for simplicity. The structure size of monolayer graphene on Cu(311) is $4.92 \text{ \AA} \times 21.44 \text{ \AA}$. The graphene lattice constant was taken 2.46 Å, adapting the lattice constants of metals accordingly to fit graphene size. The slab model consists of four Cu layers and different layers of graphene on two sides. The positions of the carbon atoms are allowed to relax.

For the grazing scattering geometry, the RCT is calculated by means of a rate equation. To calculate the population of the atomic state we integrate the rate equation along the trajectory of ion motion [32]:

$$dP/dt = \Gamma_{\text{capture}}(z)(1 - P) - \Gamma_{\text{loss}}(z)P, \quad (1)$$

where z and P are normal distance to the surface and the population of the atomic state, respectively; $\Gamma_{\text{capture}}(z) = g_{\text{capture}}\Gamma(z)F_{\text{capture}}(z)$ is the ion level width for electron capture; $\Gamma_{\text{loss}}(z) = g_{\text{loss}}\Gamma(z)F_{\text{loss}}(z)$ is the ion level width for electron loss; $F_{\text{capture}}(z)$ and $F_{\text{loss}}(z)$ are the electron capture and loss weights, respectively. The statistical factors are usually taken as $g_{\text{capture}} = 2$ and $g_{\text{loss}} = 1$ to account for the electron spin. The pseudopotential for graphene-covered surfaces was constructed from the density functional theory (DFT) calculations (see details in Ref. [42]).

The procedure of calculation of $\Gamma(z)$ as a function of the ion-surface distance is described elsewhere [43]. In brief, we perform a series of auxiliary calculations of the $\text{Na}^0 3s$ state decay in front of the metallic surface for a fixed ion-surface distance. The alkali-metal atom is considered as the hydrogen-like atom, consisting of a single *active electron* and a screened atomic core. We use the three-dimensional realization of the wave-packet propagation method [32,44–50], which considers a direct study of the evolution of the active electron wave packet in the compound potential created by the surface and the projectile. Thus, we numerically solve the time-dependent Schrödinger equation (TDSE) with known initial conditions:

$$i \frac{d\psi(\mathbf{r}, t)}{dt} = \left[-\frac{\Delta}{2} + U(\mathbf{r}, t) \right] \psi(\mathbf{r}, t), \quad \psi(\mathbf{r}, 0) = \psi_0(\mathbf{r}), \quad (2)$$

where $U(\mathbf{r}, t) = V_{e\text{-ion}}(\mathbf{r}, t) + V_{e\text{-surface}}(\mathbf{r}) + \Delta V_{e\text{-surface}}(\mathbf{r}, t)$ is the time-dependent potential felt by the active electron. $V_{e\text{-ion}}(\mathbf{r}, t)$ describes the interaction of the electron with the atomic center; $V_{e\text{-surface}}(\mathbf{r})$ represents the electron interaction with the surface; $\Delta V_{e\text{-surface}}(\mathbf{r}, t)$ accounts for the change of the electron-surface interaction.

The numerical scheme of the TDSE solver provides the time evolution of the system's wave function $\psi(\mathbf{r}, t)$. If we project the current wave function on the initial state of the system $\psi_0(\mathbf{r})$, we will obtain an autocorrelation function,

$$A(t) = \langle \psi_0(\mathbf{r}) | \psi(\mathbf{r}, t) \rangle, \quad (3)$$

which is a complex function. Its real and image parts oscillate in time with a frequency equal to the energy level of the electron, and its square of modulus is the probability that a system remains in the initial state. This means that $|A(t)|^2 = 1$ corresponds to the situation when the electron occupies the atomic level, while $|A(t)|^2 = 0$ means that the outer electron of the Na atom has completely gone into the nanosystem.

The more sophisticated interpretation of the RCT process deals with the Fourier transform of the autocorrelation function,

$$g(\omega) = \frac{1}{\pi} \int_0^\infty dt e^{i\omega t} A(t) = \frac{1}{\pi} \int_0^\infty dt e^{i\omega t} \langle \psi_0(\mathbf{r}) | \psi(\mathbf{r}, t) \rangle, \quad (4)$$

which is the complex function of oscillation frequency (electron energy). The modulus of $g(\omega)$ gives the distribution of the energy levels' occupation. In the case of nanosystems the ion occupation probability $|A(t)|^2$ oscillates in time, even for the large propagation times $|A(t)|^2 > 0$. This means that the Fourier transform of the autocorrelation function besides the main peak will contain side lobes. To suppress the side lobes we use the Hamming window,

$$g(\omega) = \frac{1}{\pi} \int_0^\infty dt e^{i\omega t} A(t) f(\omega);$$

$$f(\omega) = 0.54 - 0.46[\cos(2\pi/T_{\text{max}})], \quad (5)$$

where T_{max} is the propagation time. To extract the level width, we calculate the incline of the $\ln |A(t)|^2$ on the linear-descending section. The numerical experiments with the test data give the error estimation of the described procedure as about 2%.

IV. RESULTS AND DISCUSSION

Figure 2 shows the neutral fraction for 2–5 keV Na^+ ions scattered from different numbers of graphene layers (NL) on PC, and for HOPG and PC. The neutral fraction for the clean PC is on the order of 25%, and it decreases with increasing graphene layers, reaching a limiting value of about 3% for three to five layers, which is the same as that scattered from the HOPG surface. Moreover, the neutral fraction for Na^+ ions scattered from the monolayer graphene is obviously lower than that for PC, which contradicts our anticipation, because the monolayer graphene has a lower work function than PC.

Since the RCT depends on the ion energy level position relative to the Fermi level of the surface, we have calculated the work function for these surfaces. The calculated work functions for NL = 0–4 are shown in Fig. 3(a). The work function first decreases and then increases with increasing graphene layers. The work function of Cu(311) is 4.94 eV, and more than the experimental value of 4.6 eV for PC [51]. The work function of the monolayer graphene on Cu(311) sharply declines to 4.18 eV, which is slightly smaller than the

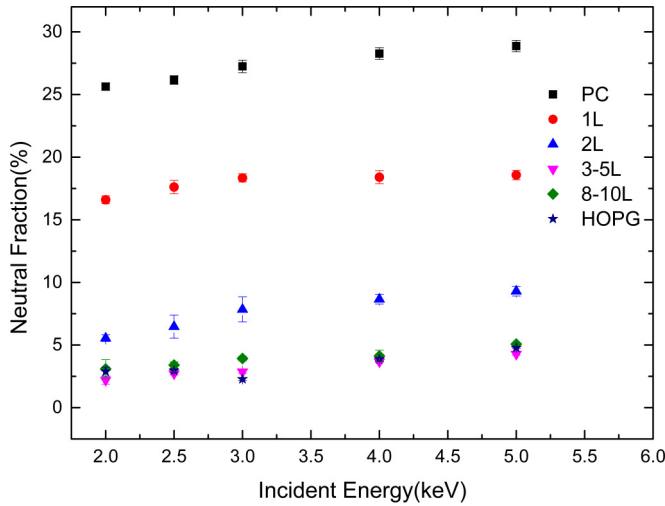


FIG. 2. Experimental neutral fractions of polycrystalline copper, different graphene layers on polycrystalline copper, and HOPG surface as a function of incident energy. The scattering angle and incident angle are 7° and 3.5° , respectively.

experimental value of 4.25 eV for the monolayer graphene on PC [51]. For $NL = 2, 3$, and 4, the work functions are 4.3, 4.46, and 4.54 eV, respectively. The work function of $NL = 4$ is almost in agreement with the calculated value of 4.52 eV and the experimental value of 4.55 eV for graphite [52].

The free-electron gas model of the RCT has been widely used to describe the neutralization of alkali-metal ions on metal surfaces [29]. The general trend is that the neutral fraction of scattered alkali-metal ions decreases exponentially

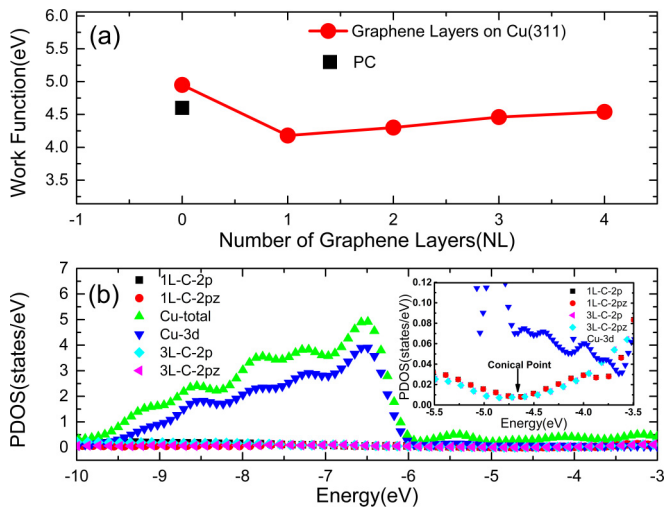


FIG. 3. (a) Red dots show the calculated work function of graphene layers on Cu(311) as a function of graphene layers, and the black square represents the experimental value of the work function of the polycrystalline copper [51]. (b) shows the PDOS of a single C atom for one- and three-layered graphene on Cu(311) and a single Cu atom for Cu(311). The right side inset shows the PDOS of a single Cu atom for Cu(311) and a single C atom for one- and three-layered graphene on Cu(311). The zero of the energy scale is set at the vacuum level.

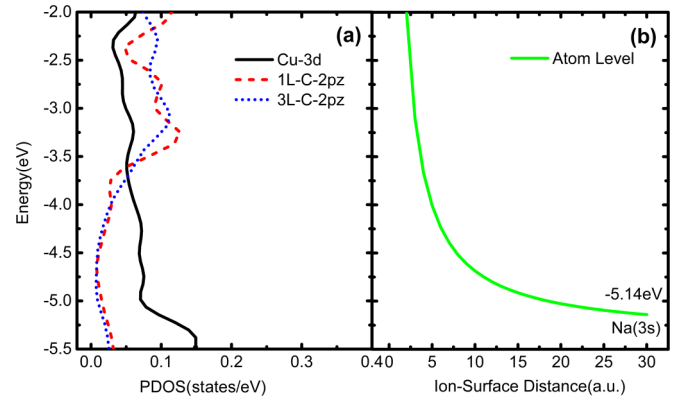


FIG. 4. (a) The PDOS of a single Cu atom for Cu(311) and a single C atom for one- and three-layered graphene on Cu(311). (b) The schematic diagram of the shifted atomic level of Na(3s) in front of the surfaces as a function of the ion-surface distance. The zero of the energy scale is set at the vacuum level.

with increasing work function. According to the calculation of the work function mentioned above, Na^+ neutral fractions gradually decrease with the increase of NL and are consistent with HOPG when $NL = 4$. This prediction has been confirmed experimentally. However, an anomaly appears here; the neutral fraction of the clean PC clearly exceeds that of the monolayer graphene, as shown in Fig. 2. Such behavior is not consistent with the free-electron-gas model prediction, according to the comparison of whatever the calculated work functions of Cu(311) are and the monolayer-graphene/Cu(311), or the experimental work functions of PC and the monolayer-graphene/PC.

It is noted that the ion level width $\Gamma(z)$, which is strongly related to the PDOS, determines the RCT efficiency or the rate of electron transfer. Figure 3(b) shows the total and partial density of states (DOS) of Cu(311) and graphene layers on Cu(311). The PDOS of $3d$ state electrons of Cu(311) is obviously larger than the $2p_z$ state electrons of the graphene located below the Fermi level, because the Cu and C atom have $3d^{10}4s^1$ and $2s^22p^2$ electronic configuration, respectively, and the number of electrons of $3d$ states for the Cu atoms is much larger than that of $2p$ states of the C atoms. One- and three-layered graphene on Cu(311) retain their unique electron structures. The inset shows the Fermi level of the monolayer graphene on Cu(311) shifts upward by 0.5 eV with respect to the conical point due to the substrate effect, which is in line with previous research findings [53,54], while the substrate effect for the three-layered graphene on Cu(311) is weakened and the upward shift of the Fermi level with respect to the conical point is reduced.

In order to qualitatively understand the reasons for the above-mentioned phenomena, the schematic diagram of the RCT process between the projectile and the surfaces with different PDOS has been shown in Fig. 4. When the atomic level of Na(3s) (first ionization potential 5.14 eV) is shifted up by the image potential, remaining below the Fermi level of the surface for large ion-surface distances, the resonant neutralization of Na^+ ions occurs, while for short distances the atomic level shifts above the Fermi level, and then the resonant ionization takes place. The levels of $3d$ and $2p_z$

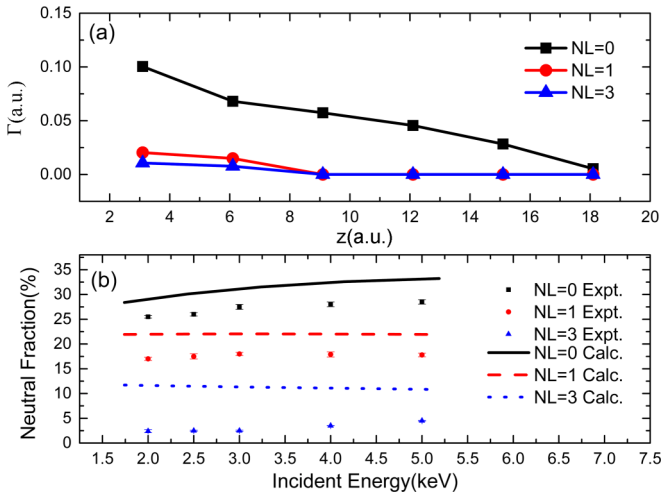


FIG. 5. (a) The energy level width of $\text{Na}(3s)$ on the surface of different graphene layers as a function of the ion-surface distance. (b) The Na^+ neutral fraction on the copper surface, covered by different numbers of graphene layers (see NL in legend). Lines correspond to calculation results and symbols to experimental results. Parameter $\text{NL} = 0$ corresponds to the clean copper surface.

orbital electrons are close to the Fermi level for Cu and C, respectively. The number of $3d$ electronic states of copper near the Fermi level is much larger than that of the $2p_z$ electronic states of carbon. Hence the RCT efficiency should decrease on the graphene surfaces.

It is necessary to obtain a key parameter of the ion level width $\Gamma(z)$ before calculating the neutral fraction using the rate equation for the outgoing trajectory of ion motion. Figure 5(a) exhibits the RCT ion level width $\Gamma(z)$ for $\text{NL} = 0, 1, \text{ and } 3$. The ion level width $\Gamma(z)$ of the clean copper surface is significantly larger than that for the graphene layers and $\Gamma(z)$ decreases with the increase of the graphene layers, which is indeed related to the quantum size effect due to their different electronic structures shown in Fig. 3(b). The RCT occurs between alkali-metal ions and electronic structure near the Fermi level, as shown in Fig. 4. In terms of the WPP method the electron motion is confined in the normal direction because of the 2D nature of graphene; then the greater $\Gamma(z)$ for clean copper can be explained by more efficient tunneling to the bulk. When an electron occupies the atoms of the top atomic layer of copper, it propagates further to “congenious” copper atoms with relatively high efficiency, while for a graphene-covered copper surface an electron initially occupies the carbon atoms; hence further propagation to “alien” copper atoms occurs less efficiently.

Figure 5(b) shows that the theoretical results qualitatively reproduce the experimental data. The neutral fraction increases with the number of graphene layers, which has the same trend as the variation of the ion level width $\Gamma(z)$ with the number of layers. The value of the Fermi level was taken as -4.5 eV for $\text{NL} = 1$, -4.7 eV for $\text{NL} = 3-5$, and -5 eV for $\text{NL} = 0$. The theoretical results reproduce the experimental data. The significant discrepancy for $\text{NL} = 3-5$ is probably related to the ion level width $\Gamma(z)$ calculation procedure, because for the extremely small Γ the WPP method

usually overestimates it. The general trend is that despite the smaller work function, the neutralization on graphene-covered copper is less efficient because the ion level width $\Gamma(z)$ for graphene-covered surfaces is much smaller than that for clean copper. The less efficient neutralization of graphene-covered surfaces can be attributed to the smaller PDOS for graphene/HOPG.

It is known that, the different extension of the electron density beyond those surfaces has influence on the $\Gamma(z)$ of scattered ions, at least for free-electron metal surfaces [55]. We have performed the molecular dynamics simulation of scattered ion trajectories using the KALYPSO software package [56], in which the Ziegler-Biersack-Littmark (ZBL) potentials are used. The closest distances were found to be 2.45 and 2.33 a.u. for 2 keV Na^+ ions scattered from copper and graphene surfaces, respectively. For the same incident energy, the trajectories on the two surfaces do not differ strongly. Although the jellium edge is located closer to the topmost layer of atoms for copper surfaces than that for graphene surfaces, the electron density penetrated by the projectile in front of the first atomic layer for copper is much higher than that for graphene surfaces. As a result, it leads to the larger $\Gamma(z)$ for copper at a given ion-surface distance, as shown in Fig. 5(a).

V. CONCLUSION

In conclusion, we have reported on the experimental and theoretical study of resonant neutralization of alkali-metal ions on clean and graphene-covered copper surfaces. This study has shown that the neutral fraction decreases as the number of graphene layers increases and that three- to five-layered graphene exhibits the same electronic structure as graphite, which reveals that the neutral fraction contains the direct information of electronic structure changing with the number of graphene layers. The anomalous phenomenon that the neutral fraction on the high work function copper surface is greater than that on the low work function graphene surface indicates that the DOS plays an important role in the RCT process, except for work function. The high DOS near the Fermi level of copper is strongly shielded by the monolayer graphene. Resonant neutralization spectroscopy based on LEIS is shown to be a promising candidate for detecting the quantum size effects corresponding to the variation of electronic structure near the Fermi level in 2D materials at an atomic layer level.

ACKNOWLEDGMENTS

The authors are very grateful to Prof. Philippe Roncin for careful reading and comments, and to Yachao Zhu, Yin Li, and Xin Zhang for their help in the initial stages of the experiment. This work was supported by the National Natural Science Foundation of China (Grants No. 11405078 and No. 11474140), the Russian Foundation for Basic Research (Grant No. 20-02-00577), and Key Laboratory of Special Function Materials and Structure Design, Ministry of Education (lzujbky-2021-kb06).

- [1] B. Anasori, M. R. Lukatskaya, and Y. Gogotsi, *Nat. Rev. Mater.* **2**, 16098 (2017).
- [2] F. Bonaccorso, L. Colombo, G. Yu, M. Stoller, V. Tozzini, A. C. Ferrari, R. S. Ruoff, and V. Pellegrini, *Science* **347**, 1246501 (2015).
- [3] P. Niu, L. L. Zhang, G. Liu, and H. M. Cheng, *Adv. Funct. Mater.* **22**, 4763 (2012).
- [4] Y. Cao, V. Fatemi, S. Fang, K. Watanabe, T. Taniguchi, E. Kaxiras, and P. J. Herrero, *Nature (London)* **556**, 43 (2018).
- [5] F. Shahzad, M. Alhabeab, C. B. Hatter, B. Anasori, S. M. Hong, C. M. Koo, and Y. Gogotsi, *Science* **353**, 1137 (2016).
- [6] L. Britnell, R. M. Ribeiro, A. Eckmann, R. Jalil, B. D. Belle, A. Mishchenko, Y. J. Kim, R. V. Gorbachev, T. Georgiou, S. V. Morozov, A. N. Grigorenko, A. K. Geim, C. Casiraghi, A. H. Castro Neto, and K. S. Novoselov, *Science* **340**, 1311 (2013).
- [7] D. J. Late, B. Liu, H. S. S. Ramakrishna Matte, V. P. Dravid, and C. N. R. Rao, *ACS Nano* **6**, 5635 (2012).
- [8] C. Ma, M. G. Ma, C. L. Si, X. X. Ji, and P. B. Wan, *Adv. Funct. Mater.* **31**, 2009524 (2021).
- [9] L. Tong, Z. R. Peng, R. F. Lin, Z. Li, Y. L. Wang, X. Y. Huang, K. H. Xue, H. Y. Xu, F. Liu, H. Xia, P. Wang, M. S. Xu, W. Xiong, W. D. Hu, J. B. Xu, X. L. Zhang, L. Ye, and X. S. Miao, *Science* **373**, 1353 (2021).
- [10] H. Tsai, F. Liu, S. Shrestha, K. Fernando, S. Tretiak, B. Scott, D. T. Vo, J. Strzalka, and W. Nie, *Sci. Adv.* **6**, eaay0815 (2020).
- [11] F. Dixit, K. Zimmermann, R. Dutta, N. J. Prakash, B. Barbeau, M. Mohseni, and B. Kandasubramanian, *J. Hazard. Mater.* **423**, 127050 (2022).
- [12] G. Cao, *Nanostructures and Nanomaterials: Synthesis, Properties and Applications*, 2nd ed. (Imperial College Press, London, 2004).
- [13] L. Liu, S. Ryu, M. R. Tomasik, E. Stolyarova, N. Jung, M. S. Hybertsen, M. L. Steigerwald, L. E. Brus, and G. W. Flynn, *Nano Lett.* **8**, 1965 (2008).
- [14] N. Jung, N. Kim, S. Jockusch, N. J. Turro, P. Kim, and L. Brus, *Nano Lett.* **9**, 4133 (2009).
- [15] X. Zubizarreta, E. V. Chulkov, I. P. Chernov, A. S. Vasenko, I. Aldazabal, and V. M. Silkin, *Phys. Rev. B* **95**, 235405 (2017).
- [16] A. H. M. Abdul Wasey, S. Chakrabarty, and G. P. Das, *J. Appl. Phys.* **117**, 064313 (2015).
- [17] H. H. Brongersma, M. Draxler, M. de Ridder, and P. Bauer, *Surf. Sci. Rep.* **62**, 63 (2007).
- [18] D. Kunwar, S. Zhou, A. DeLaRiva, E. J. Peterson, H. Xiong, X. I. Pereira-Hernández, S. C. Purdy, R. ter Veen, H. H. Brongersma, J. T. Miller, H. Hashiguchi, L. Kovarik, S. Lin, H. Guo, Y. Wang, and A. K. Datye, *ACS Catal.* **9**, 3978 (2019).
- [19] X. He, W. Zhou, Z. Y. Wang, Y. N. Zhang, J. Shi, R. Q. Wu, and J. A. Yarmoff, *Phys. Rev. Lett.* **110**, 156101 (2013).
- [20] A. M. Belu, D. J. Graham, and D. G. Castner, *Biomaterials* **24**, 3635 (2003).
- [21] R. McAdams, *Rev. Sci. Instrum.* **85**, 02B319 (2014).
- [22] S. Henderson *et al.*, *Nucl. Instrum. Methods Phys. Res., Sect. A* **763**, 610 (2014).
- [23] T. E. Moore, D. J. Chornay, M. R. Collier, F. A. Herrero, J. Johnson, M. A. Johnson, J. W. Keller, J. F. Laudadio, J. F. Lobell, K. W. Ogilvie, P. Rozmarynowski, S. A. Fuselier, A. G. Ghielmetti, E. Hertzberg, D. C. Hamilton, R. Lundgren, P. Wilson, P. Walpole, T. M. Stephen, B. L. Peko *et al.*, *Space Sci. Rev.* **91**, 155 (2000).
- [24] J. A. Yarmoff, Y. Yang, and Z. Sroubek, *Phys. Rev. Lett.* **91**, 086104 (2003).
- [25] G. F. Liu, P. Karmakar, and J. A. Yarmoff, *Phys. Rev. Lett.* **98**, 176104 (2007).
- [26] G. F. Liu, Z. Sroubek, and J. A. Yarmoff, *Phys. Rev. Lett.* **92**, 216801 (2004).
- [27] P. Karmakar, G. F. Liu, Z. Sroubek, and J. A. Yarmoff, *Phys. Rev. Lett.* **98**, 215502 (2007).
- [28] Y. Yang and J. A. Yarmoff, *Phys. Rev. Lett.* **89**, 196102 (2002).
- [29] H. Winter, *Phys. Rep.* **367**, 387 (2002).
- [30] A. G. Borisov, D. Teillet-Billy, J. P. Gauyacq, H. Winter, and G. Dierkes, *Phys. Rev. B* **54**, 17166 (1996).
- [31] C. Meyer, F. Bonetto, R. Vidal, E. A. García, C. Gonzalez, J. Ferrón, and E. C. Goldberg, *Phys. Rev. A* **86**, 032901 (2012).
- [32] P. Y. Liu, L. Y. Yin, Z. Zhang, B. Ding, Y. Q. Shi, Y. Li, X. Zhang, X. X. Song, Y. L. Guo, L. Chen, X. M. Chen, I. K. Gainullin, and V. A. Esaulov, *Phys. Rev. A* **101**, 032706 (2020).
- [33] L. Gao, Y. C. Zhu, Y. Q. Shi, P. Y. Liu, Y. Q. Xiao, G. P. Li, Y. R. Liu, V. A. Esaulov, X. M. Chen, L. Chen, and Y. L. Guo, *Phys. Rev. A* **96**, 052705 (2017).
- [34] Y. Yang, Z. Sroubek, and J. A. Yarmoff, *Phys. Rev. B* **69**, 045420 (2004).
- [35] F. Varchon, R. Feng, J. Hass, X. Li, B. N. Nguyen, C. Naud, P. Mallet, J.-Y. Veuillen, C. Berger, E. H. Conrad, and L. Magaud, *Phys. Rev. Lett.* **99**, 126805 (2007).
- [36] R. S. Gao, P. S. Gibner, J. H. Newman, K. A. Smith, and R. F. Stebbings, *Rev. Sci. Instrum.* **55**, 1756 (1984).
- [37] H. C. Straub, M. A. Mangan, B. G. Lindsay, K. A. Smith, and R. F. Stebbings, *Rev. Sci. Instrum.* **70**, 4238 (1999).
- [38] N. Takahashi, Y. Adachi, M. Saito, and Y. Haruyama, *Nucl. Instrum. Methods Phys. Res., Sect. B* **315**, 51 (2013).
- [39] A. Gupta, G. Chen, P. Joshi, S. Tadigadapa, and P. C. Eklund, *Nano Lett.* **6**, 2667 (2006).
- [40] G. Kresse and J. Furthmüller, *Phys. Rev. B* **54**, 11169 (1996).
- [41] G. Kresse and D. Joubert, *Phys. Rev. B* **59**, 1758 (1999).
- [42] I. K. Gainullin, *Phys. Rev. A* **95**, 052705 (2017).
- [43] I. K. Gainullin and M. A. Sonkin, *Phys. Rev. A* **92**, 022710 (2015).
- [44] V. A. Ermoshin and A. K. Kazansky, *Phys. Lett. A* **218**, 99 (1996).
- [45] A. G. Borisov, A. K. Kazansky, and J. P. Gauyacq, *Phys. Rev. Lett.* **80**, 1996 (1998).
- [46] E. Yu. Usman, I. F. Urazgil'din, A. G. Borisov, and J. P. Gauyacq, *Phys. Rev. B* **64**, 205405 (2001).
- [47] H. Chakraborty, T. Niederhausen, and U. Thumm, *Phys. Rev. A* **69**, 052901 (2004).
- [48] H. Chakraborty, T. Niederhausen, and U. Thumm, *Phys. Rev. A* **70**, 052903 (2004).
- [49] I. K. Gainullin, *Comput. Phys. Commun.* **210**, 72 (2017).
- [50] I. K. Gainullin and M. A. Sonkin, *Comput. Phys. Commun.* **188**, 68 (2015).
- [51] A. Siokou, F. Ravani, S. Karakalos, O. Frank, M. Kalbac, and C. Galiotis, *Appl. Surf. Sci.* **257**, 9785 (2011).
- [52] S. Mammadov, J. Ristein, J. Krone, C. Raidel, M. Wanke, V. Wiesmann, F. Speck, and T. Seyller, *2D Mater.* **4**, 015043 (2017).

- [53] G. Giovannetti, P. A. Khomyakov, G. Brocks, V. M. Karpan, J. van den Brink, and P. J. Kelly, *Phys. Rev. Lett.* **101**, 026803 (2008).
- [54] P. A. Khomyakov, G. Giovannetti, P. C. Rusu, G. Brocks, J. van den Brink, and P. J. Kelly, *Phys. Rev. B* **79**, 195425 (2009).
- [55] Y. Bandurin, V. A. Esaulov, L. Guillemot, and R. C. Monreal, *Phys. Rev. Lett.* **92**, 017601 (2004).
- [56] M. A. Karolewski, *Instrum. Methods Phys. Res., Sect. B* **230**, 402 (2005).